Invited Chapter in *Automation, Miniature Robotics and Sensors for Non-Destructive Testing and Evaluation*, Y. Bar-Cohen Editor, April 99

5.1 CONVENTIONAL ACTUATORS, SHAPE MEMORY ALLOYS, AND ELECTRORHEOLOGICAL FLUIDS

Constantinos Mavroidis, Charles Pfeiffer and Michael Mosley
Robotics and Mechatronics Laboratory
Department of Mechanical and Aerospace Engineering
Rutgers University, The State University of New Jersey
98 Brett Rd., Piscataway, NJ 08854-8058
mavro@jove.rutgers.edu, cpfeiffe@caip.rutgers.edu, mjmosley@jove.rutgers.edu
Tel: 732 - 445 – 0732, Fax: 732 - 445 - 3124

5.1 CONVENTIONAL ACTUATORS, SHAPE MEMORY ALLOYS, AND ELECTRORHEOLOGICAL FLUIDS 1
5.1.1 INTRODUCTION 1
5.1.2 CONVENTIONAL ACTUATORS 2
5.1.2.1 Hydraulic Actuators 2
5.1.2.1.1 Principle of Operation 2
5.1.2.1.2 Advantages - Disadvantages 3
5.1.2.2 Pneumatic Actuators 4
5.1.2.2.1 Principle of Operation 4
5.1.2.2.2 Advantages - Disadvantages 5
5.1.2.3 Electric Actuators 6
5.1.2.3.1 Principle of Operation 6
5.1.2.3.2 Advantages - Disadvantages 8
5.1.3 SHAPE MEMORY ALLOY ACTUATORS 10
5.1.3.1 History of SMA 10
5.1.3.2 Principle of Operation 10
5.1.3.3 Nickel-Titanium (Ni-Ti) Shape Memory Alloy 13
5.1.3.4 Shape Memory Alloy Actuators in Robotic Applications 14
5.1.3.5 Modeling, Dynamics, and Control of Shape Memory Alloy Actuators 19
5.1.4 ELECTRO-RHEOLOGICAL FLUIDS (ERF) 22
5.1.5 REFERENCES 24

5.1.1 INTRODUCTION

Robots, being an evolution of machines and mechanisms, originated by the ancient Greeks, Alexandrian and Roman engineers [Dimarogonas, 1993]. The first machines were simple jointed mechanisms that were actuated by human operators. The incorporation of an energy source, other than the human, to actuate and move certain components of the machine was a very important step towards automation of motion. Perhaps one of the earliest "roboticists" was the great Greek engineer and inventor Ctesibios (ca. 283-247 B.C.) who applying a knowledge of pneumatics and hydraulics invented the precision clock. Heron of Alexandria (ca. 1st century A.D.) building on Ctesibios' work, wrote the fundamental textbook *On Automatic Theaters, On Pneumatics and On Mechanics,* that is considered as the first well documented robotic system description outside of mythology [Rosheim, 1994]. After this time, machines, mechanisms and robotic technology has evolved considerably during the roman and medieval times, the renaissance and industrial revolution and modern era.

From the mechanical point of view, a robotic system is a mechanism composed of a set of links connected with joints that transfer motion and force from an input source to an output end-effector location. Different types of actuators have been used as input motion and force sources. Hydraulic, pneumatic and electric actuators are called "conventional" because they are used by the majority of robotic and automated mechanical systems. Recently, many new types of actuators are being used to provide the necessary motion and force input. Examples of these actuators are Shape Memory Alloys, Electro-Rheological Fluids, Magneto-Active Transducers, Piezoelectric Motors and Electroactive Polymers. The goal of this chapter is to review the properties of conventional actuators and describe the function of several non-conventional actuators.

5.1.2 CONVENTIONAL ACTUATORS

Three main types of actuation have been the core of motion and force power for all robotic systems. They are Hydraulic, Pneumatic, and Electric motors. These three come from two main types of power conversion. The first two are considered fluid machines in that they use fluid to create mechanical motion whereas the electric motor converts electrical energy into mechanical energy. The following will describe briefly, each actuation method with its advantages and disadvantages. Detailed description of these actuators can be found in many robotics and haptics textbooks such as [Stadler, 1995; Burdea, 1996]. A very good comparative study of actuators is robotics can be found in [Hollerbach, Hunter and Ballantyne, 1992].

5.1.2.1 Hydraulic Actuators

5.1.2.1.1 Principle of Operation

An actuator of this type works by changes of pressure. This system can be used in both linear and rotary actuation. The general linear mechanism consists of a piston encased in a chamber with a piston rod protruding from the chamber. The piston rod serves as the power transmission link between the piston inside the chamber and the external world. There are two major configurations of this actuator: single or double action. For the single action configuration, it can exert controllable forces in only one direction and uses a spring to return the piston to the neutral or un-energized position. Figure 1 shows a cut away view of a double action actuator which can be actively controlled in both directions within the chamber. In the case of rotary actuation, the power unit is a set of vanes attached to a drive shaft and encased in a chamber. Within the chamber the actuator is rotated by differential pressure across the vanes and the action is transmitted through the drive shaft to the external world.

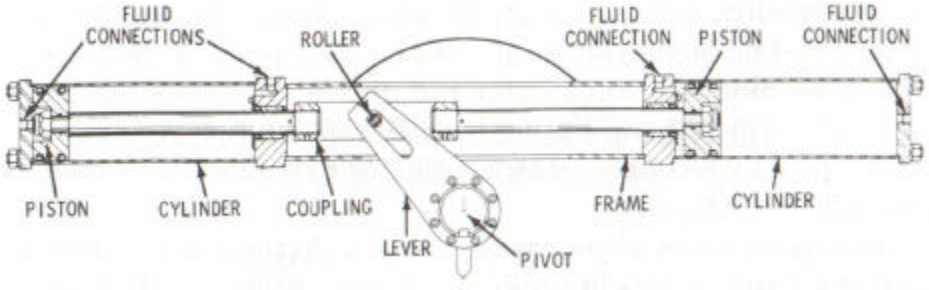

Figure 1: Drawing of Double Action Hydraulic Actuator
[Stewart, 1987, pg. 55; Reprinted by permission of Macmillan Publishing]

A representative closed loop position control for a linear hydraulic actuator is shown in Figure 2. The open loop dynamics of the hydraulic actuator are usually approximated with a first order system where the time constant depends on the piston area A. The desired piston position X_d is compared to the actual position X. The obtained error E is processed by the controller which in most of the cases is a PID controller and the drive current I which will be the input to the servo-valve is obtained. Then the current I is multiplied with the flow gain K_q and the servo-valve no-load flow Q_0 is obtained. The Output Flow Q is the difference between Q_0 and a flow Q_d due to disturbance forces F_d which are mainly friction and gravity. Flow Q is the input to the hydraulic system that will result in a piston velocity V and a piston displacement X.

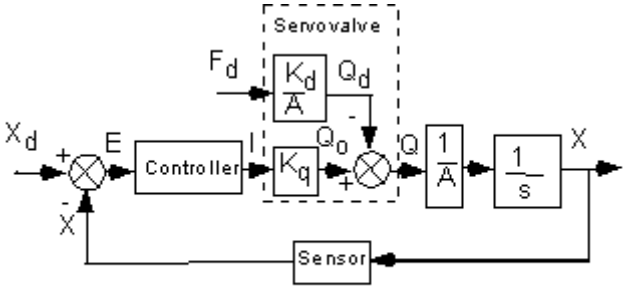

Figure 2: Closed Loop Position Control of a Hydraulic Actuator

It has to be noted that in Figure 2, the dynamics of the servo-valve have been approximated with very simple linear relationships. This representation can be realistic in low frequency operations. However, in high frequencies, electro-hydraulic servo-valves can exhibit highly non-linear dynamics. [Hollerbach, Hunter and Ballantyne, 1992].

Hydraulic manipulators are mainly used in applications where large robotic systems with high payload capability are needed. Examples are nuclear and underwater applications. A hydraulic manipulator that is currently used in many different heavy duty industrial and field tasks is shown in Figure 3. The TITAN 3 by ALSTOM Automation Schilling Robotics [Schilling, 1999] is extensively used for underwater applications on remotely operated vehicles (ROVs). The seven-function TITAN 3 has the dexterity and accuracy necessary to perform the fine movements needed for complex tasks. When this ability is combined with the manipulator's reach (1,915 mm or 75.4 inches), payload capacity (113 kg at full extension), depth rating (available up to 6,500 msw), and large operating envelope, the TITAN 3 offers unequaled performance in a wide range of subsea applications. The TITAN 3 is constructed primarily of titanium for structural strength, light weight, and corrosion resistance.

5.1.2.1.2 Advantages - Disadvantages

One of the main advantages of hydraulic actuators is that these systems can deliver a great deal of power compared to their actuator inertia. Other aspects, which make a hydraulic actuator useful are the low compressibility of hydraulic fluids and, the high stiffness which leads to an associated high natural frequency and rapid response. This means that the robot using hydraulic actuators can execute very quick movements with great force. Additionally they tend to be reliable and mechanically simplistic as well as having a low noise level, and relatively safe

during operation. As for this method of actuation, design characteristics are well known so the process of design is made easier due to this extent of knowledge.

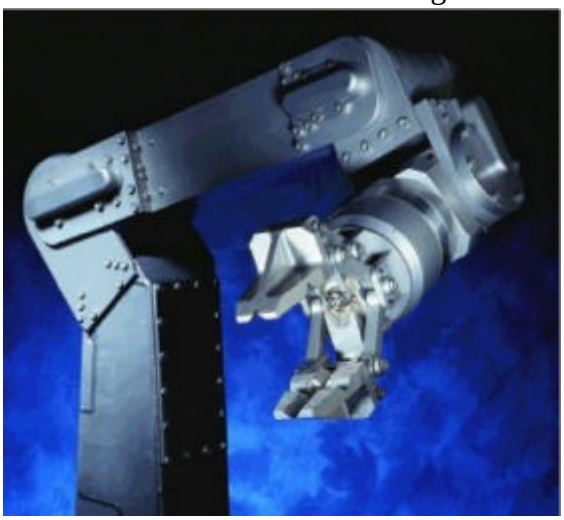

Figure 3: Schilling TITAN 3 Manipulator [Schilling, 1999]
[Reprinted by permission of Schilling]

One of the larger concerns with hydraulic systems is the containment of the fluid within the actuation system. Not only is this because of the contamination of the surrounding environment, but the leakage can also contaminate the oil and possibly lead to damage of interior surfaces. Additionally, the hydraulic fluid is flammable and pressurized so leaks could pose an extreme hazard to equipment and personnel. This adds the undesirable aspect of additional maintenance to maintain a clean sealed system. Other drawbacks include lags in the control of the system due to the transmission lines and oil viscosity changes from temperature. In fact, such temperature changes in the fluid can be drastic enough to form vapor bubbles when combined with the changes in fluid pressure in a phenomena called cavitation. During operation as temperature and pressure fluctuate, these bubbles alternately form and collapse. At times, when a vapor bubble is collapsing, the fluid will strike interior surfaces which had vapor filled pores and high surge pressures will be exhibited at the bottom of these pores. This bubble collapsing can dislodge metal particles in the pore area and leave a metallic suspension within the fluid. The degradation of the interior surfaces and the contamination of the fluid result in a marked drop in the performance of the system.

5.1.2.2 Pneumatic Actuators

5.1.2.2.1 Principle of Operation

These type of actuators are the direct descendents of the hydraulic systems. The difference between the two is that pneumatic systems use a compressible gas (i.e. air) as the medium for energy transmission. This makes the pneumatic system more passively compliant than the hydraulic system. With pneumatic actuators, the pressure within the chambers is lower than that of hydraulic systems resulting in lower force capabilities. In Figure 4 there is a cut away view of the basic pneumatic actuator. It is quite similar to the hydraulic counterpart however there are no return hydraulic lines for fluid. In a typical actuator of this type the fluid, namely air, is simply exhausted through the outlet valve in the actuator. Digital control of

pneumatic systems is very similar to hydraulics with some exceptions to gains and stiffness constants (see also Figure 2.)

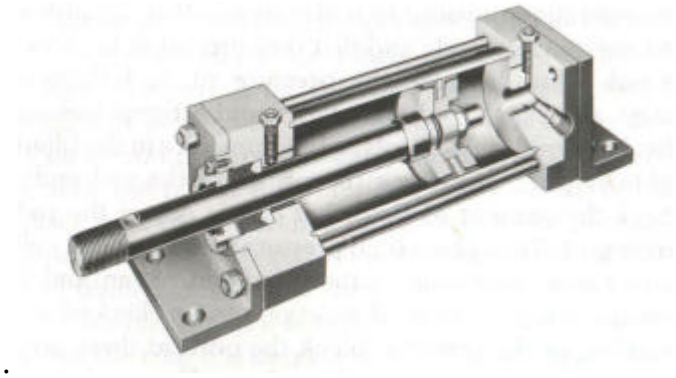

Figure 4: Cutaway View of Pneumatic Actuator
[Stewart, 1987, pg. 316; Reprinted by permission of Macmillan Publishing]

Pneumatic systems have been used in robotic systems when lightweight, small size systems are needed with relatively high payload to weight ratio. Examples of applications include walking machines and haptic systems. In Figure 5, a six-legged, pneumatically powered walking robot is shown [Binnard, 1995]. The pneumatic actuation system provides lightweight, powerful actuators. The robot's mechanical structure is a lightweight frame built from carbon fiber and aluminum tubing and injection molded plastic. Preliminary results indicate that Boadicea walks faster, and can carry more payload, than previous small walkers. Boadicea has six legs powered by compressed air at 100 psi.

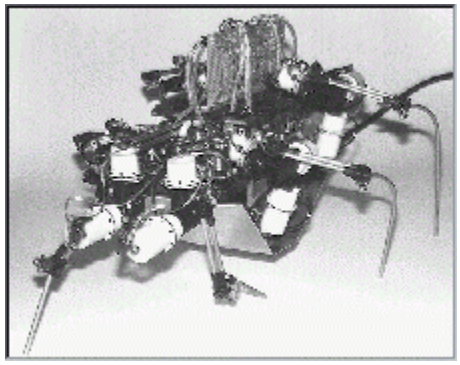

Figure 5 – Boadicea: a Six-Legged Pneumatic System
[Binnard, 1995; Reprinted by Permission of MIT]

5.1.2.2.2 Advantages - Disadvantages

Pneumatic actuators have less force capability than hydraulic actuators. Since, in contrast, the system operates at a lower pressure than the hydraulics and does not require return lines for the fluid, the support structure of the manipulator is much lighter than the other system. Pneumatics are cleaner and nonflammable which makes its uses in certain environments (i.e. – cleanrooms, operating rooms) more desired. Additionally, installation, operation and maintenance is easier and cost is lower.

Though the lack of hydraulic fluid makes this system cleaner, it has the disadvantage of not having a self-lubricating actuator. This generally means that pneumatic systems have a high friction force to overcome in order to maneuver and the diversion of power to combat friction gives these systems a lower working force. The release valve that allows pressurized air to escape has a tendency to be load if a muffler is not employed. Of course due to the medium which is compressible, control of motion is handled differently than hydraulics. While compliance is desired in a hydraulic system, force and speed are wanting in a pneumatic setup therefore the methodology to get these performance aspects is left to ingenuity of software control and nozzle design.

5.1.2.3 Electric Actuators

5.1.2.3.1 Principle of Operation

Of the three types of conventional actuator systems, electric motors have the largest variety of possible devices such as: Direct Current (DC) motors and their variants (brushed and brushless, low inertia, geared and direct drive, permanent magnet), Alternate Current (AC) motors, Induction Motors, and Stepping Motors. By definition, the principle behind an electric motor is a simple one, which is the application of magnetic fields to a ferrous core and thereby inducing motion.

A schematic of an AC motor and of a two-pole induction motor is shown in Figure 6 and of a DC motor in Figure 7 [Henkenius, 1991]. An AC motor is comprised of an electromagnet positioned above a permanent magnet which is mounted on a pivot. When current is sent through the coil, the permanent magnet rotates so that opposite poles align. As the AC current switches direction, the permanent magnet continues rotation to align with reversed poles.

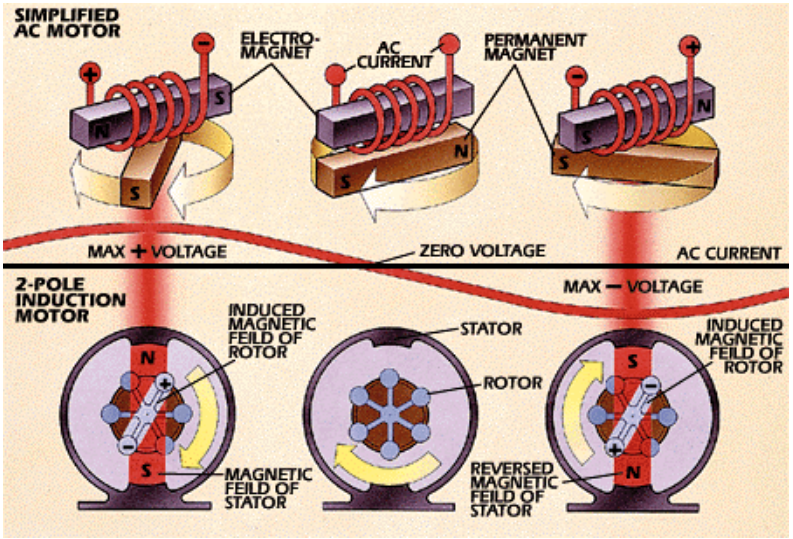

Figure 6: Basic Operation of a DC induction motor [Henkenius, 1991]
[Reprinted by Permission of Popular Mechanics]

A two-pole induction motor, shown in Figure 6, has a rotor which is the inner part that rotates and a stator of a permanent magnet composed of two or more permanent magnet pole pieces. The rotor is composed of windings which are connected to a mechanical commutator.

The opposite polarities of the energized winding and the stator magnet attract and the rotor will rotate until it is aligned with the stator. Just as the rotor reaches alignment, the brushes move across the commutator contacts and energize the next winding. Notice that the commutator is staggered from the rotor poles. If the connections of a motor are reversed, the motor will change directions. DC motors are very similar to induction motors. The only difference is that a current is sent to the armature through contact between brushes and commutator. Spinning commutator acts as a reversing switch that alternates magnetic field.

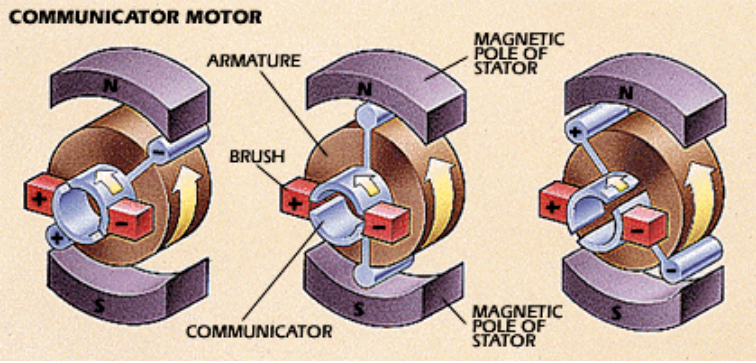

Figure 7: Block diagram of a DC motor [Henkenius, 1991]
[Reprinted by Permission of Popular Mechanics]

A position control scheme, in the Laplace domaine, for a permanent magnet DC motor is shown in Figure 8. The desired motor position Θ_d (and velocity) is compared to the actual position Θ (and velocity) that is usually obtained using angular position sensor such as optical encoders or potensiometers. This comparison yield the position (and velocity) error E that is processed by the controller. Usually, a PID controller is used and is designed to achieve fast and accurate response with no overshoot. The output of the controller is the voltage V that will be the input to the DC motor. Voltage V will be reduced by the "back emf" voltage V_b which is created by the angular motion of the motor shaft. The back emf voltage is proportional to the angular velocity Ω and the coefficient of this linear relationship is called the "back emf constant" K_b. The open loop dynamics of the motor are distinguished into the dynamics of the electrical part and of the mechanical part. The electrical circuit dynamics are approximated using a first order system where L is the armature inductance and R is the armature resistance. The armature current I which is the output of the electrical part, will result in the motor torque τ_m. The relationship between I and τ_m is linear and the coefficient K_i of this linear relationship is called the "motor constant". The sum of the motor torque τ_m with the disturbance torques τ_l felt by the motor shaft will be the input to the mechanical part of a DC motor. The disturbance torques τ_l are due to the load carried by the motor, friction and elastic effects at the payload level and other dynamic effects that have not been taken into account by the model. The coefficient n is the gear ratio and divides any torques due to the payload. The dynamics of the mechanical part are of second order, including a motor inertia J_m and a friction term with friction coefficient B_m. A detailed description of the control of a DC motor can be found in [Spong and Vidyasagar, 1989].

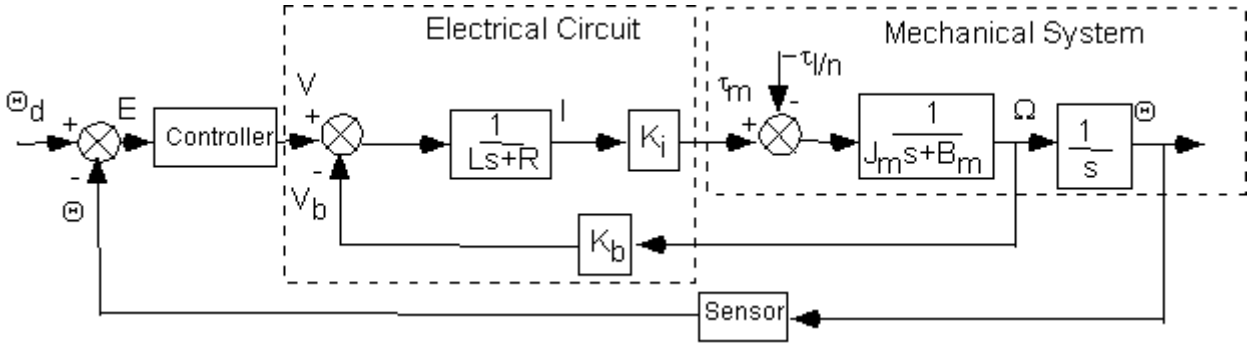

Figure 8: Position Control of a DC Motor

5.1.2.3.2 Advantages - Disadvantages

Since the energy medium for electric motors is easily stored and re-supplied by recharging batteries if mobility is needed, this makes electric motors the best choice when it comes to portability. Concurrently, as far as energy mediums, electric motors' power source is more adaptable to environments than hydraulics or pneumatics since volumetrically they take up less space. There are no hydraulic return lines, air lines, high pressure pumps, or reservoir tanks as in the case of the previously described systems. In tasking a robot to perform difficult maneuvers, the flexibility of control of the mechanical system with electric motors is far greater. This is because of the energy medium can be used by both the control system and the manipulator directly. They are also easy to install, clean (no leaks) and relatively quiet when they are compared to the hydraulic and pneumatic actuators.

The major disadvantage of electrical motors is that they produce very small torques compared to their size and weight. As the trend in robotics is to build smaller robots that are very powerful, electrical motors seem to be not suitable for such applications. Table 1 gives a broad scope view of the three types of conventional actuators studied in this section. Figure 9 compares the power density versus the weight of several conventional actuators and of the Shape Memory Alloy actuators that are discussed in the next section.

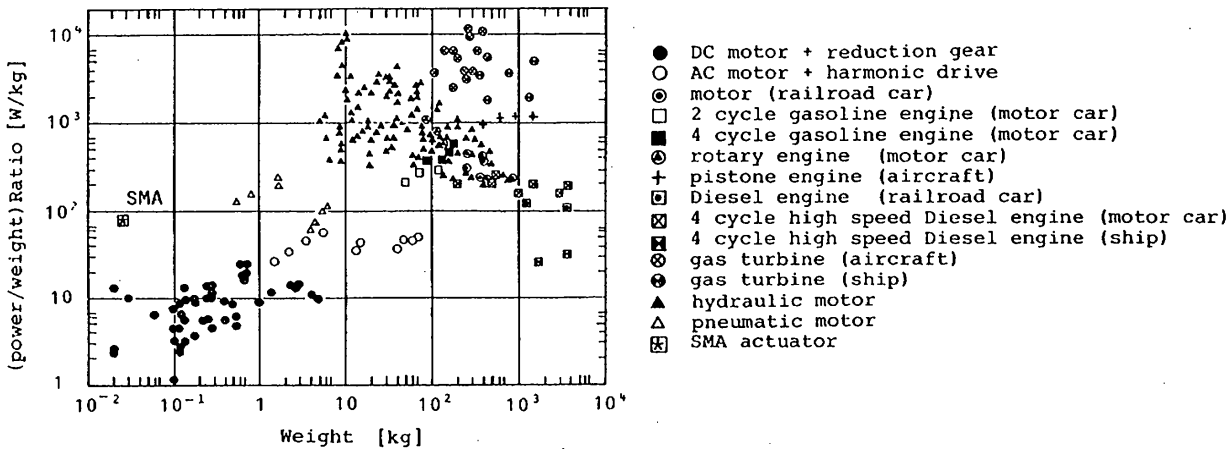

Figure 9: Power Density vs. Weight of Several Actuators [Hirose et al., 1989a]
[Reprinted by Permission of VSP]

Table 1: Comparison of Conventional Actuators, [Adapted from Zeldman,1984]
[Reprinted by Permission of Marcel Dekker, Inc.]

FACTOR	ELECTRICAL	HYDRAULIC	PNEUMATIC
1. Basic System	Solid State Logic, Power Amplifiers, DC or AC Motors, Gear Boxes, Ball Nuts, Coolers	Pump, Sump, Regulators (Pressure, Temp., Flow), Filters, Heat Exchangers, Servo Valves, Motors, Actuators, Accumulators	Compressor, Interstage Coolers, Pressure Controls, Filter, Dryers, Mufflers, Valves, Actuators, Snubbers
2. Working Principle	Electricity	High Quality Oil Base with Additives, Water Based Solutions, Synthetic Liquids	Air, Nitrogen, Combustion Products
3. Efficiency	Over 90% for Large Systems	Seldom over 60%	Seldom over 30%
4. Susceptability to Contamination	*Low:* (Electrical Line Noise +/- 10%) Easily Handled RFI Noise Easily Handled by Shielding and Filtration	*High:* Filters Required Special Handling During Maintenance. Cleaning Procedures Important. Servo Valves Easily Damaged	*Intermediate:* Less Trouble Than Oil. Particles Drop Out Before Getting To Valves. Moisture & Corrosion A Problem.
5. Weight to Force Ratio	*Poor:* Motor & Gearing Must Be Carried By Each Sub-system. Poorest Weight to Force Ratio	*Excellent:* Highest Force to Weight Ratio	*Fair:* Light Weight, But Low Pressures Produce Intermediate Force to Weight Ratio
6. Safety of Operation	Safest System Electrical Shock Hazard & Grounding Must Be Considered	Leakage of Flammable Fluids & Fire Hazards High Velocity Jets of Fluid Can Pierce Skin, Blood Poisoning Eye Inflammations Possible	Flying Debris From Ruptures can be Very Dangerous. Explosions Possible When Volatile Oils Are Present (Nitrogen Non-Explos.)
7. Temperature Sensitivity and Heat Removal	Low Temperature Sensitivity in the Operating Range, but Poor Heat Dissipation Relative to Hydraulic	High Temperature Sensitivity Due to Viscosity Changes. Differential Thermal Expansion Can Cause Transient Malfunctions. Excellent Heat Removal at Remote Heat Exchangers	Low Temperature Sensitivity. Differential Thermal Expansion Can Cause Transient Difficulties. Heat Removal is not Normally a Problem Since Systems Vent To Atmosphere
8. Input Power Supply	24 Volts to 460 Volts	50-5000 PSI	5-500 PSI
9. Load Variation Susceptability	Dry Friction On Output Motors Can Cause Small to Intermediate Steady State Errors at Null	Dry Friction On Outputs Can Cause Small Steady State Errors Around Null	Serious Steady State Errors Can Occur Around Null Position Due To Dry Friction On Output Shaft
10. System Stiffness	Reasonably Stiff-Stiffness Dependent on Speed Reduction Concepts	The Stiffest, Most Responsive System for Heavy Loads	Very Soft System (Hydraulic is 400 x Stiffer)

5.1.3 SHAPE MEMORY ALLOY ACTUATORS

5.1.3.1 History of SMA

In 1932, a Swedish physicist by the name of Arne Olander discovered an interesting phenomenon when working with an alloy of gold (Au) and cadmium (Cd). The Au-Cd alloy could be plastically deformed when cool and then be heated to return to, or "remember", the original dimensional configuration. This phenomenon is known as the Shape Memory Effect (SME) and the alloys that exhibit the behavior are called Shape Memory Alloys (SMA). In 1958, researchers Chang and Read demonstrated the Shape Memory Effect at the Brussels World's Fair. Specifically, they showed that the SME could be used to perform mechanical work by cyclically lifting a weight using a Au-Cd SMA. Further research revealed other materials that demonstrate this phenomenon. In 1961, a group of U. S. Naval Ordnance Laboratory researchers lead by William Beuhler stumbled across a significant discovery in the field of SME and SMA. While testing an alloy of Nickel and Titanium for heat and corrosion resistance, they found that it too exhibited the SME. The Ni-Ti SMA proved to be significantly less expensive, easier to work with, and less dangerous (from health standpoint) than previously discovered alloys. These factors refreshed interest and research in the Shape Memory Effect and its applications. [Toki Corporation, 1987; Grant, 1995]

Researchers, designers, and companies recognized the potential to use the SME in engineering applications. As a result, starting in the 1970's, commercial products began to appear. For the most part, the early devices functioned as fasteners and took advantage of a single shape memory dimensional change. Some examples of these static devices are couplings for piping systems and electrical connectors. Next, researchers began to propose SMA devices to perform dynamic tasks; thus, they began to play the role of actuators. In order to perform a dynamic task, the SMA must experience a cycle of heating, cooling, and deformation. This requirement led some companies, such as Delta Metal in England, to use SMA actuators in temperature regulation systems where the environmental temperature could be used for thermal actuation. Delta Metal proposed that SMA devices could be used to automatically open and close greenhouse windows, operate valves that control building temperatures, and control automobile fan clutches. In 1982, Sharp incorporated SMA actuators into electric oven dampers and in 1983, Matsushita Electric designed SMA actuated louvers for air conditioners [Toki Corporation, 1987]. Other researchers pursued electricity (resisitive or joule heating) as a source of heat and thus actuation. In 1971, a team lead by Sawyer developed and tested an artificial heart powered by electrical actuation of SMA elements. In 1983, Honma, Miwa, and Iguchi [Honma et al, 1989] showed that SMA actuation could be controlled by resistive heating and proposed that SMA actuators could be used in micro-robotics. Research concerning the application and control of SMA actuators in robotic systems has continued and expanded through the present.

5.1.3.2 Principle of Operation

Shape Memory Alloys consist of a group of metallic materials that demonstrate the ability to return to some previously defined shape or size when subjected to the appropriate thermal procedure. Some examples of these alloys are Ag-Cd, Au-Cd, Cu-Al-Ni, Cu-Sn, Cu-Zn-(X), In-Ti, Ni-Al, Ni-Ti, Fe-Pt, Mn-Cu, and Fe-Mn-Si. The SME occurs due to a temperature

and stress dependent shift in the material's crystalline structure between two different phases called martensite and austenite. Martensite, the low temperature phase, is relatively soft whereas Austenite, the high temperature phase, is relatively hard. For a simple example of the SME in action, consider the following. If a straight bar of some SMA in its austenitic (high temperature) phase is allowed to cool below the phase transition temperature, the crystalline structure will change to martensite. If the bar is subsequently plastically deformed, by say bending, and then reheated above the phase transition temperature, it will return to its original straight configuration. In order to understand this phenomenon, it is useful to consider the highly simplified two-dimensional representation of the material's crystalline arrangement shown in Figure 10.

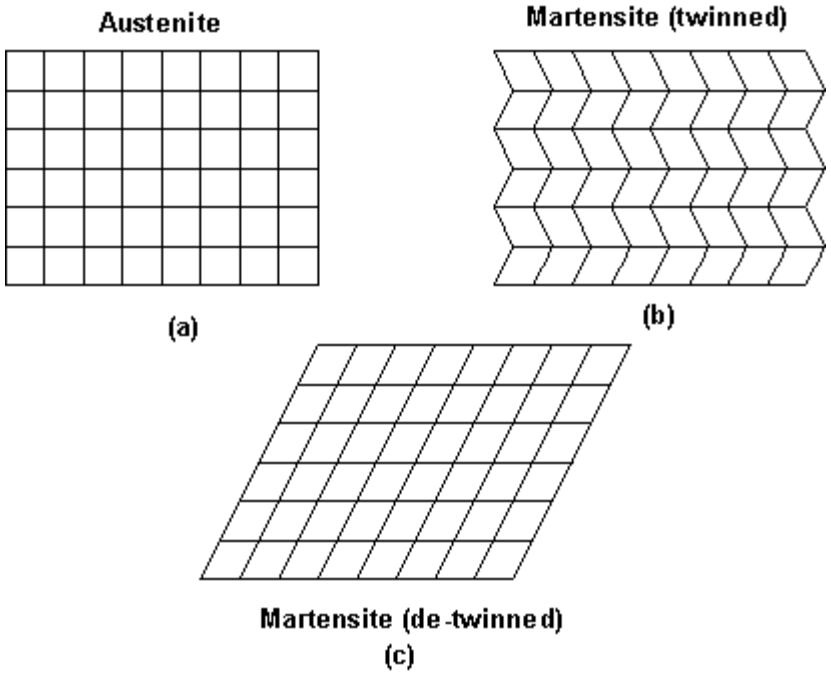

Figure 10: Material Crystalline Arrangement During the Shape Memory Effect

Each box represents a grain of material with its corresponding grain boundaries. The grains form a heavily twinned structure, meaning they are oriented symmetrically across grain boundaries. The twinned structure allows the internal lattice of individual grains to change while still maintaining the same interface with adjacent grains. As a result, Shape Memory Alloys can experience large macroscopic deformations while maintaining remarkable order within its microscopic structure. For example, if a piece of SMA starts as austenite (Figure 10a), the internal atomic lattice of each grain is cubic creating grains with more or less right angles. If it is now allowed to cool below the phase transition temperature, the crystalline structure changes to martensite (Figure 10b) and the grains collapse to the structure represented by the diamonds. Note that the grains lean in different directions for different layers. Now, if sufficient stress is applied, the martensitic structure represented in Figure 10b will start to yield and "de-twin" as the grains re-orient such that they are all aligned in the same direction (see Figure 10c). This behavior can be better understood by examining a typical stress-strain curve for the martensite phase (Figure 11). For small stresses, the structure represented in Figure 10b behaves elastically (region 0 to 1). At 1, the material yields and de-twinning occurs between 1 and 2. At 2, the martensitic structure is entirely de-twinned as represented by Figure 10c. Now, a second elastic

region occurs from 2 to 3. At 3, permanent plastic deformation begins that is not recoverable by the SME.

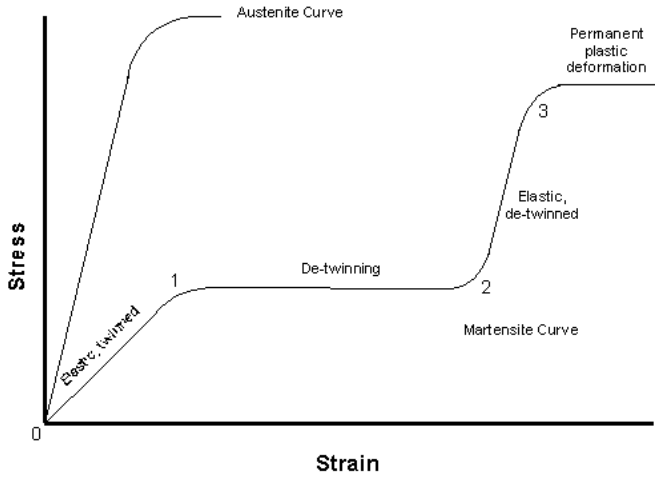

Figure 11: Stress -Strain Relationship of a Shape Memory Alloy

The change that occurs within a SMA's crystalline structure during the SME is not a thermodynamically reversible process. In other words there is energy dissipation due to internal friction and creation of structural defects. As a result, a temperature hysteresis occurs which is illustrated in Figure 12a. Starting at 1, the material is 100% martensite. During heating, the martensite/austenite composition follows the lower curve. When the temperature reaches A_S, austenite begins to form. Austenite continues to form until temperature A_F is reached and the material is 100% austenite. If cooling occurs from 2, the material composition follows the upper curve. When the temperature drops to M_S, martensite begins to form and continues to form until temperature M_F is reached. Now the material is back to its starting condition – 100% martensite. This temperature hysteresis translates directly into hysteresis in the strain/temperature relationship (see Figure 12b). The hysteresis behavior makes it challenging to develop modeling and control schemes for a SMA actuator. For a given SMA, the hysteresis is dependent on the composition of the alloy and the manufacturing processes. Most Shape Memory Alloys have a hysteresis loop width of 10 to 50°C, with the exception of some wide hysteresis alloys used for joining applications such as couplings [Waram, 1993]. Additional information on the priniple of operation of SMA's can be found in [Toki Corporation, 1987; Waram, 1993].

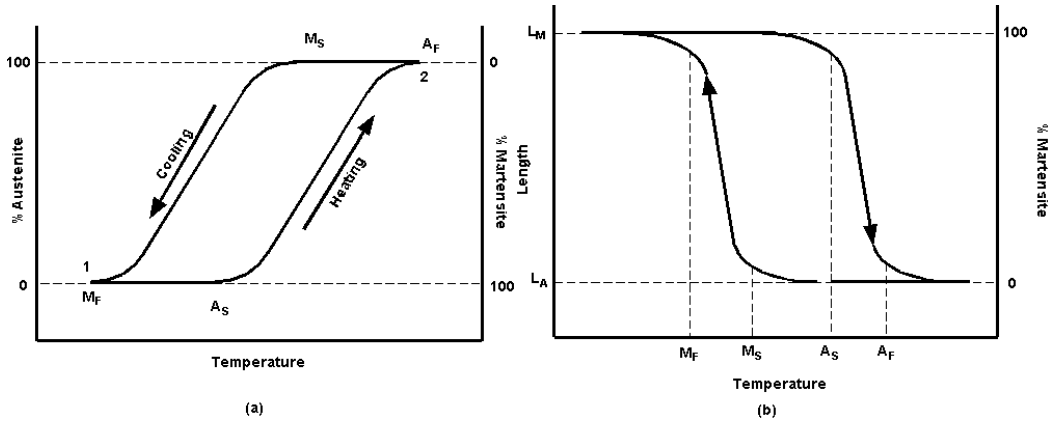

Figure 12: Hysteresis Loops in Shape Memory Alloys

5.1.3.3 Nickel-Titanium (Ni-Ti) Shape Memory Alloy

Out of all the Shape Memory Alloys that have been discovered so far, Nickel-Titanium (Ni-Ti) has proven to be the most flexible and beneficial in engineering applications. The following characteristics of Ni-Ti make it stand out from the other SMA's: greater ductility, more recoverable motion, excellent corrosion resistance (comparable to series 300 stainless steels), stable transformation temperatures, high biocompatability, and the ability to be electrically heated for shape recovery [Waram, 1993].

Ni-Ti SMA is the binary, equiatomic intermetallic compound of nickel and titanium. In simpler words it is approximately 50 atomic% Ni and 50 atomic% Ti. The beneficial characteristics of the intermetallic compound are a moderate solubility range for excess Ni or Ti, as well as for most other metallic elements, and a ductility comparable to most ordinary alloys. The solubility allows Ni-Ti to be alloyed with other elements to change the mechanical properties and phase transformation temperature (here, phase transformation temperature is taken to mean A_F). For example, adding additional Ni to the binary compound (up to 1% extra) strongly depresses the phase transformation temperature and increases the yield strength of the austenite. Iron and chromium can also be added to lower the transformation temperature. By varying these and other elements the transformation temperature can be varied from –200 to 110°C (-325 to 230°F). Copper can be added to decrease the hysteresis and lower the deformation stress (detwinning stress) of the martensite. Table 2 shows the key physical properties of equiatomic Ni-Ti SMA [Hodgson et al., 1998].

Table 2: Physical Properties of Ni-Ti

Property	Austenite	Martensite
Melting Temperature, °C (°F)	1300 (2370)	
Density, g/cm^3 (lb$_m$/in^3)	6.45 (0.233)	
Resistivity, μΩ-cm	Approx. 100	Approx. 70
Thermal Conductivity, W°C/cm (BtuHr°F/ft)	18 (10)	8.5 (4.9)
Corrosion Resistance	Similar to 300 series stainless steel or titanium alloys	
Young's Modulus, GPa (1000 ksi)	Approx. 83 (12)	Approx. 28 to 41 (4 to 6)
Yield Strength , Mpa (ksi)	195 to 690 (28 to 100)	70 to 140 (10 to 20)
Ultimate Tensile Strength, MPa (ksi)	895 (130)	
Transformation Temperatures, °C (°F)	-200 to 110 (-325 to 230)	
Latent Heat of Transformation, KJ∗atom/kg (cal∗atom/g)	167 (40)	
Shape Memory Strain	8.5% maximum	

Manufacturing Ni-Ti SMA and shaping it for a specific purpose is not a simple task. Since Ti is a very reactive element, melting must be done in an inert atmosphere. Common methods are plasma-arc melting, electron-beam melting, and vacuum induction melting. Ni-Ti

ingots can be initially shaped using standard hot-forming and cold-working processes. During cold-working the alloy work hardens very quickly and must be annealed frequently. Work hardening and the correct heat treatment can be used to improve the SMA's performance by reducing the stress needed to de-twin the martensite and increasing the strength in the austenite phase. Machining Ni-Ti through cutting methods is difficult, as is welding, brazing, and soldering. Grinding, shearing, and punching are often better methods to create specific shapes. The "memory configuration" of a SMA part is defined by restraining the part in the desired shape, and then heat treating at typically 500 to 800°C (950 to 1450°F) [Hodgson et al., 1998]. Companies such as Dynalloy, Inc. and Shape Memory Applications, Inc. provide prefabricated SMA elements such as wire, rod, ribbon, strip, sheet, and tubing. Additionally, they are able to create custom elements to user specifications.

5.1.3.4 Shape Memory Alloy Actuators in Robotic Applications

Using Shape Memory Alloy actuators provides an interesting alternative to conventional actuation methods. Their advantages create a means to drastically reduce the size, weight, and complexity of robotic systems. First of all, SMA actuators possess an extremely high force to weight ratio. A Ni-Ti actuator can apply an actuation stress of 500 MPa (72.5 ksi). So, a 150 μm diameter Ni-Ti wire can apply a force of 8.8 N which is 0.897 kg_f (1.99 lb_f). If the wire is 10 cm (3.94 in.) long it would weigh 11.4 mg (0.025 lb_m) and could contract 0.85 cm. So, the actuator can lift an object 78,000 times its own weight nearly 1 cm! Granted a simple electrical circuit is needed to heat the wire, but the force to weight ratio is still remarkable. Shape Memory Alloy actuators also are incredibly compact and simple. In the example described above, the actuator itself has a volume of only 0.002 cm^2. A SMA actuation system consists only of the SMA element and a heating and cooling method. The cooling method can be as simple as a combination of natural convection, conduction, and radiation. A final advantage is noiseless operation. Whereas conventional actuators produce a significant amount of noise, the SMA actuator is completely silent.

Shape Memory Alloy actuators do have disadvantages which must be thoroughly considered and analyzed prior to deciding to use SMA for an application. First of all, they operate with a low efficiency. A SMA actuator is effectively a heat engine where the material converts thermal energy directly into work. Therefore, the efficiency of the actuator cannot be greater than that of the Carnot cycle. The efficiency of the Carnot cycle is low in the temperatures where typical SMA actuator operate -- not exceeding 10% [Hirose, Ikuta, and Umetani, 1984]. Second, SMA actuators operate at a low bandwidth, meaning they are relative slow to cycle. The cycling time is primarily dependent on the heat transfer characteristics of the SMA "cooling system". The primary parameters that affect bandwidth are the temperature and type of surrounding medium, the convection of the surrounding medium, and the surface to volume ratio of the SMA elements. Depending on the environment, heat dissipation can be a problem. For a high temperature, low convection environment, the heat transfer to the surrounding medium is reduced resulting in a lower bandwidth. For a low temperature or high convection environment, the heat transfer is improved and bandwidth is increased. However, greater heat transfer also means that more power is needed to achieve actuation temperature. Another disadvantage of SMA actuators is the small absolute strains achieved by the SMA material. With only 8.5% strain available (for Ni=Ti), mechanisms actuated by SMA that are required to create large motions must be cleverly designed. Converting small motions into large motions comes with the unavoidable reduction in mechanical advantage. A final disadvantage,

and topic of much research, is the difficulty controlling SMA actuators. The Shape Memory Effect is a highly non-linear phenomenon. Non-linearities enter the process through the hysteresis behavior described earlier, non-linear heat transfer, and any non-linear change in the parameters that affects the phase composition of the material (temperature, stress). Another control issue is that the entire deflection of a SMA element occurs over a small temperature range making accurate control in partial contraction difficult. Control is also difficult due to the structural elasticity of SMA actuators.

When designing a Shape Memory Alloy actuator for a mechanism, one of the first decisions is specifying the source of heat to actuate the SMA element. In certain specialized applications, the temperature of the surrounding medium can be used as a source of heat. This method provides a excellent option when designing mechanisms that regulate temperature. For example, a SMA element can be placed in a medium (say air) whose temperature needs to be controlled. The SMA element can be manufactured such that its actuation temperature corresponds to some critical temperature of the medium. When the medium reaches the critical temperature, the SMA element would actuate and possibly open a valve supplying more cooling. Here, the SMA element acts as both the sensor and the actuator. No electronics are needed in this incredibly simple system.

For other applications, the typical source of heat to achieve actuation temperature is joule heating by electric current. The electrical source can be either DC or AC. If AC, it should be at a frequency significantly higher than the bandwidth of the SMA actuated system to avoid displacement fluctuations. The current I that flows through a SMA element with resistance R, due to a certain voltage drop V and the corresponding power P can be found from the following well-known relationships:

$$I = \frac{V}{R} \tag{1}$$

$$P = IV \quad \text{or} \quad P = I^2 R \tag{2}$$

Integrating a plot of power versus time and then dividing by the total time provides the average power. The average power required to achieve actuation temperature can be supplied by a steady or time varying signal. An example of a time varying signal that has been used extensively in electrical actuation is Pulse Width Modulation (PWM). The advantage of this method is more uniform heating of the SMA element. As expected, larger voltages/currents cause more rapid actuation.

Shape Memory Alloy material can be formed into almost any shaped actuator imaginable. All that is needed is a heat treatment process to define the actuators dimensional configuration in the austenite (actuated) phase. Some shapes that have been used are cantilever beams, wires, springs, ribbon, strip, sheet, and tubing. Although a SMA actuator could be designed such that it applies a force in three dimensions (depending on which direction it was deformed from the memory configuration), the great majority of SMA actuators apply a one directional tensile force and cannot directly apply a compressive force. In order to apply a compressive force, the actuator dimensions would have to be large enough to ensure rigidity and prevent buckling. As discussed earlier, large dimensions would cause a major decrease in the surface to volume ratio and, consequently, bandwidth. The end result is in order to have a SMA actuator with sufficient bandwidth, the SMA element must be thin, making it only capable of

applying tensile forces. Since most mechanisms require cyclic motions, a bias force is needed to return the mechanism in the opposite direction from which it was pulled by the SMA actuator. This bias force can be supplied by stored potential energy (gravity or a spring) or be provided by another SMA actuator working antagonistically. Simple examples of bias force are shown in Figure 13. Some excellent basic design principals for single element SMA Actuators can be found in [Waram, 1993].

The very simple mechanisms in Figure 13 can achieve only small linear motions. In order to achieve large motions, a SMA actuator must be cleverly attached to the mechanism it operates. For a simple mechanism consisting of a moving link that pivots about a fixed revolute joint, the small linear displacements of a SMA actuator can be converted into large angular motions by fixing one end of the actuator and attaching the free end to the moving link close to the center of rotation of the revolute joint. This is very similar to the way biological muscles move the links that make up the body. Of course, mechanical advantage is lost as the free end of the actuator approaches the center of rotation. Figure 14 shows a schematic of one way to achieve large angular deflections from a SMA actuator.

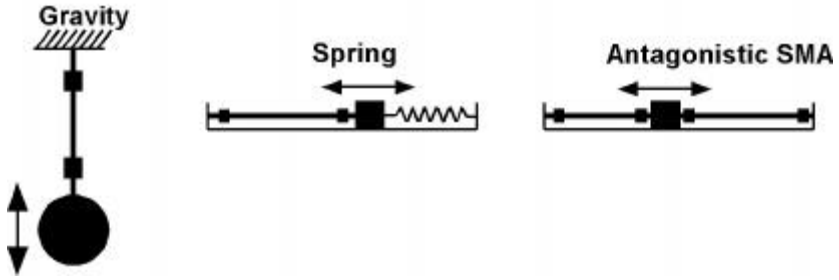

Figure 13: Examples of Bias Forces in SMA Actuated Systems

If the SMA actuator pulls on a small, flexible cable that wraps around and fastens to a pulley fixed to the moving link, the relationship between the required pulley radius, R_p, the maximum SMA deflection, Δ_{SMA}, and the desired angular deflection of the moving link, Θ, is:

$$R_p = \frac{\Delta_{SMA}}{\Theta} \tag{3}$$

Clearly from this relationship, for large angular deflections, R_p must typically be small compared to the length of the moving link, M. Considering a static problem, the resulting ratio of required actuation force, F_{SMA}, to the load, F_L is:

$$\frac{F_{SMA}}{F_L} = \frac{\Theta M}{\Delta_{SMA}} \tag{4}$$

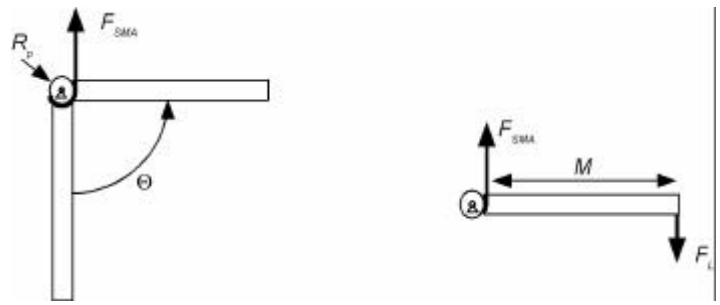

Figure 14: Large Angular Deflections from a SMA Actuator

Hirose et al., 1989b, sought to improve the torque performace of this basic mechanism by using non-circular pulleys.

Equation (4) clearly shows that if SMA actuators are used in macro-robotic systems with revolute joints, the large angular motion requirement is satisfied by attaching the SMA actuator closer to the revolute joint axis. However, as shown in this equation, this attachment creates the need for large linear forces to be applied by the SMA actuators. It is clear that using thicker wires or connecting many wires mechanically in parallel in a "bundle" will increase the force capabilities of the SMA actuator. However, the actuator bandwidth and power supply requirements may be dramatically affected by such an arrangement and have to be taken into account when designing an SMA bundle actuator. This design problem motivated Mosley, Mavroidis and Pfeiffer, 1999, and Mosley and Mavroidis, 1999, to develop and test a SMA actuator that could apply large forces (up to 100 lb_f), retain an acceptable bandwidth, and use a reasonable power supply. The experimental set-up to test this actuator is shown in Figure 15.

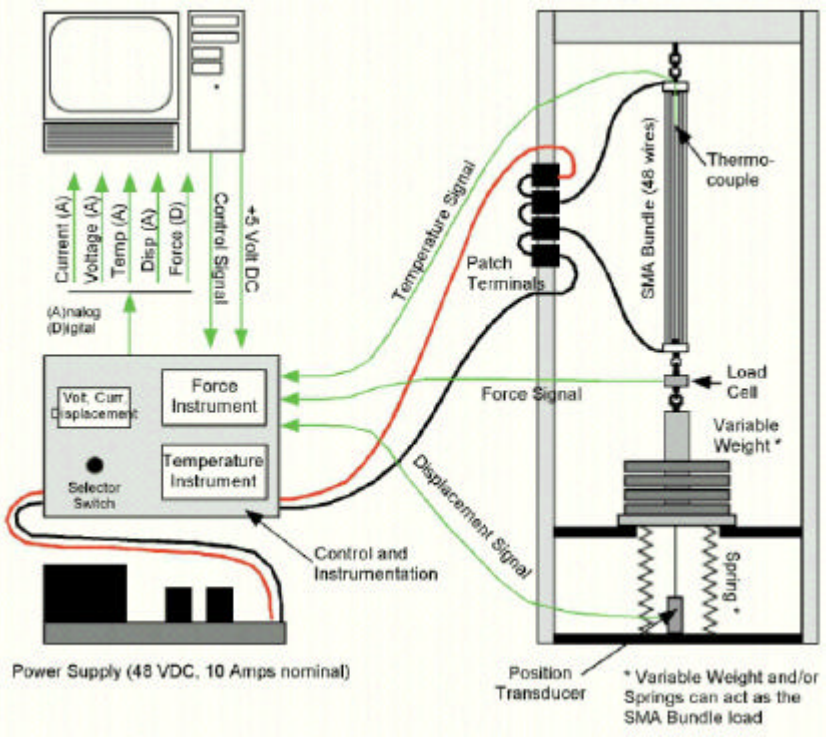

Figure 15: SMA Bundle Experimental Set-Up

The actuator used 48, 150 μm Ni-Ti wires mechanically connected in parallel with space between the wires to improve heat transfer and bandwidth. In order to avoid the low electrical resistance and corresponding high current requirement that would result from all 48 wires in a parallel circuit, the wires were connected in a combination of series and parallel current paths. This resulted in a bundle actuation current of 3.2 amps and voltage of 36.6 volts. Hirose et al., 1984, designed an actuator that used four SMA elements mechanically connected in parallel and electrically connected in series. If a bundle with a large number of wires were connected in series, the actuation voltage becomes prohibitively high.

In order to determine the performance characteristics of the wire bundled SMA actuator, an instrumented test rig, shown in Figure 15, was designed and constructed. This setup was

equipped with a load cell, linear displacement sensor, current and voltage sensors, and a thermocouple central to the bundle. Open loop experiments were conducted on the SMA bundle with two different weights and four different inputs: step, ramp, sinusoid and half sinusoid. A representative response is presented in Figure 16 where a step input is applied to the actuator lifting a load of 11lb. .

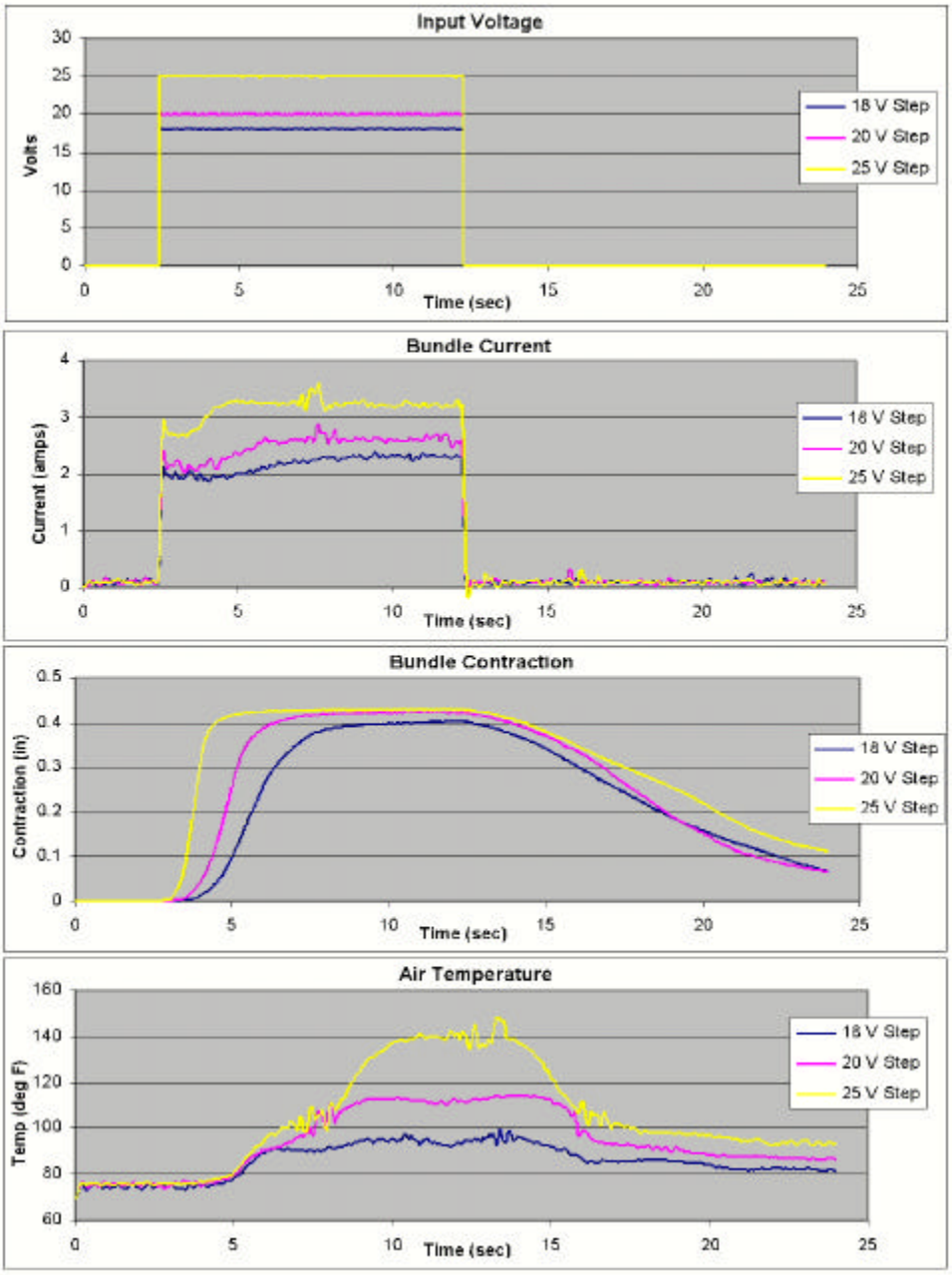

Figure 16: Step Input Signal, 11 lb. Load

Four different parameters were experimentally measured during the experiments: SMA bundle voltage drop, SMA bundle current, SMA bundle contraction, and air temperature at the center of the bundle. These tests showed interesting non-linear dynamic characteristics of the actuator. An important observation made during the dynamic analysis was the unpredictability of

the actuator's response when low to moderate voltages are applied. This characteristic strongly suggests chaotic behavior of the actuator, which could potentially cause control difficulties in fine and high accuracy tasks. An investigation into chaos was conducted using time histories, phase plots, and Poincaré maps [Mosley and Mavroidis, 1999]. As it was shown in this paper, system response to larger input voltages is periodic, whereas lower input voltages produce responses that strongly indicate chaotic behavior.

5.1.3.5 Modeling, Dynamics, and Control of Shape Memory Alloy Actuators

Developing a mathematical model that captures the behavior of a Shape Memory Alloy as it undergoes temperature, stress, and phase changes is a complicated and challenging problem. Researchers continue to study how best to model and control actuators that use this unique family of materials. As discussed earlier, it is the significant hysteresis loop that causes the problems. Gorbet and Wang, 1998, provide an excellent summary of SMA actuator modeling efforts to date. Some researchers have chosen to greatly simplify the material's behavior by creating dynamic model where the phase transition temperature is the same for heating and cooling, completely ignoring the effects of the large hysteresis. Kuribayashi, 1986, took the next step and developed a linear first-order model that estimates the hysteresis in the stress-strain behavior.

To improve the accuracy, the model must be non-linear. The complete model must capture the major hysteresis loop that occurs for changes from 100% martensite to 100% austenite and vice versa as well as the minor hysteresis loops that occur in between. Minor hysteresis loops are inherent in position control systems where heating and cooling cycles back and forth as the control system holds the actuator at the desired position. Ikuta et al., 1991, developed a novel "variable sublayer model" where, at a given time, the percentages of the different phases (including the intermediary Rhonbohedral phase) are mathematically described. As a result, for a given load, strain in the wire can be calculated from corresponding weightings of the respective strains of the different phases. Ikuta's work provided a basis for all non-linear models to date. To fully understand Ikuta's modeling process, one should consult [Ikuta et al., 1991]. A basic description is provided below.

The "variable sublayer model" for Ni-Ti SMA is developed in three steps: (1) modeling the mechanical properties of the three independent phases, (2) modeling the thermoelastic transformation, and (3) combining steps one and two creating the "variable sublayer model." The material is modeled as three layers connected in parallel representing the three different phases that can be present in the material at any given time (see Figure 17).

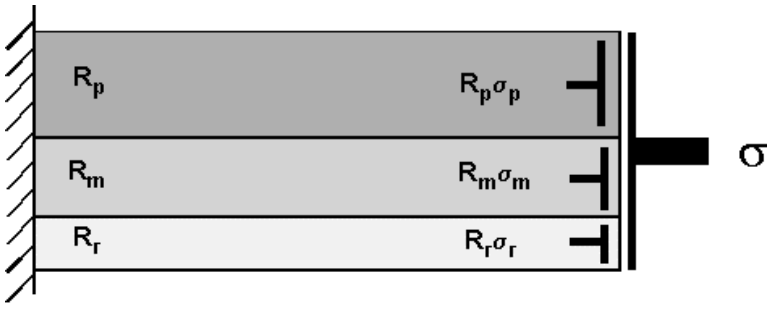

Figure 17: A Three Layer Representation of an SMA

The thickness of each layer corresponds to the volume fraction of the phase at a given moment. The total stress is a sum of the stresses in each layer weighted by the volume fraction. Resistivity of the material is modeled similar to stress – the total effective resistivity is the sum of the resistivities of each phase, each weighted by the volume fraction. Schematics of modeling the mechanical properties are shown in Figure 18. The austenite phase (often referred to as the parent phase or P-phase) is modeled as a simple elastic body. The martensite phase (M-phase) and the Rhomohedral phase are both represented as a serial connection of an elastic and plastic element. The thermoelastic transformation, including minor hysteresis loops, is mathematically modeled by a form of a "logistic curve" where the equation gives phase volume fraction as a function of temperature and stress. Ikuta compared his model to experimental results and showed greatly improved accuracy compared to previous models.

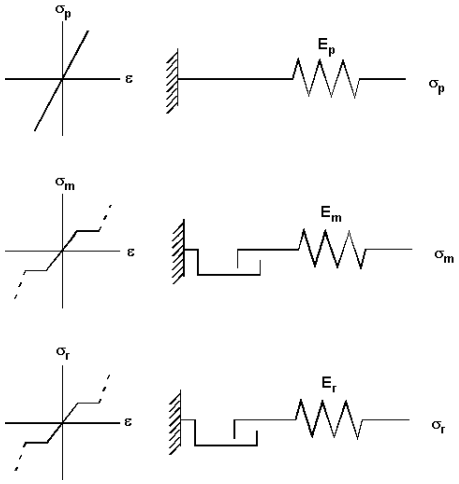

Figure 18: Models of Three Phases

Madill and Wang, 1998, developed extensions to the Ikuta's variable sublayer model that refined the modeling of the minor hysteresis loops making it more suitable for dynamically modeling position control systems where electricity is the source of heating. Their model consisted of two key elements – a temperature-current and a strain-temperature relationship. The temperature-current relationship was used to capture the dynamics of a Ni-Ti SMA actuator. The form of this relationship is a differential equation in terms of temperature, electrical current, and time:

$$rcV\frac{dT}{dt} = Ri^2(t) - hA(T(t) - T_\infty) \tag{5}$$

Where: r is the density of SMA material, c is the specific heat capacity of SMA material, V is the volume of SMA material, T is the wire temperature, t is the time, I is the current, R is the electrical resistance, h is the convection heat transfer coefficient, A is the surface area of SMA material, T is the ambient temperature.

The strain-temperature relationship, used to model hysteresis, involves two steps. First temperature and stress must be related to phase composition. Second phase composition to must be related to strain. The resulting equations are somewhat lengthy and one must consult reference [Madill and Wang, 1998] for a full explanation. The first step, relating temperature and stress to volume fraction of martensite, takes the following form:

$$R_m(q;t) = \begin{cases} \dfrac{R_{ma}^C(t)}{[1+e^{k_m^C(q-b^C)}]} + R_m^C(t), & \textit{when cooling} \\ \dfrac{R_{ma}^H(t)}{[1+e^{k_m^H(q-b^H)}]} + R_{mb}^H(t), & \textit{when heating} \end{cases} \tag{6}$$

where R_m is the martensite fraction; q is the difference between the wire temperature T and the ambient temperature $T_¥$; k_m is a temperature constant; R_{ma} and R_{mb} are constants that define the martensite fraction at the beginning and the end of the minor loops; the superscripts C and H denote cooling and heating respectively. Temperature and stress enter the equations in the exponential terms. The four functions, *R(t)*, are piecewise constant functions of time which model the minor hysteresis loops. These functions remain constant during a period of heating or cooling. However, when a shift occurs from heating to cooling or vice versa, the functions change. Here is where the primary difference occurs between this model and that of Ikuta. Ikuta's modeling of minor hysteresis loops relied on empirically determining constant parameters for each minor loop, instead of time varying functions, making it unsuitable for modeling closed loop control systems where minor loops are occurring continuously. The second step, relating phase composition to strain, takes the following form:

$$e = \begin{cases} \dfrac{s}{[E_a-(E_a-E_m)R_m]}, & 0 \le e < e_m^y \\ \dfrac{s+R_m(E_T-E_m)e_m^y}{[E_a-(E_a-E_T)R_m]}, & e_m^y \le e < e_m^d \\ \dfrac{s+R_m[(E_T-E_m)e_m^y+(E_d-E_T)e_m^d]}{[E_a-(E_a-E_d)R_m]}, & e_m^d < e \end{cases} \tag{7}$$

where e is the tensile strain; s is the tensile load (Mpa); s_a and s_m stress [Mpa] due to 100% austenite and martensite respectively; E_a, E_m, E_T, E_d, the elasticity [Mpa] of austenite, fully twinned martensite, partly twinned martensite and detwinned martensite; e_m^y yield strain of twinned martensite; e_m^d minimum strain of detwinned martensite; R_m martensite fraction.

Madill and Wang, 1998, tested their model against results of both open and closed loop experiments. The correlation between the model and the experimental results was excellent for the open loop testing as well as for closed loop testing with a proportional gain controller. The correlation was very close for a PI controlled closed loop experiment.

Very little work has been performed in the control of SMA actuated robotic systems. This is a very difficult problem to solve for three main reasons: a) SMA actuators present non-linear dynamics where classical linear controllers can not be used; b) the response of the system is highly dependent on temperature changes; and c) the SMA actuators present an unpredictability in small voltages. This sensitivity in initial condition at low inputs, suggest chaotic behavior which means that if high accuracy tasks are needed, then conventional controllers won't be able to achieve the desired accuracies. Nevertheless, there were some very important results after applying several controllers. Classical PI, PD and PID controllers have been studied by [Madill and Wang, 1998; Reynaerts and Van Brussel, 1991; Ikuta et al., 1988]. A PI controller including a temperature feedback has been studied by [Troisfotaine, Bidaud and Dario, 1997]. A variable structure controller has been studied by [Grant 1995; Grant and Hayward, 1997].

5.1.4 ELECTRO-RHEOLOGICAL FLUIDS (ERF)

Electro-Rheological fluids (ERFs) are fluids that experience dramatic changes in rheological properties in the presence of an electric field (see Figure 19). Willis M. Winslow first explained the effect in the 1940s using oil dispersions of fine powders [Winslow, 1949]. The fluids are made from suspensions of an insulating base fluid and particles on the order of one tenth to one hundred microns in size. The electro-rheological effect, sometimes called the *Winslow* effect, is thought to arise from the difference in the dielectric constants of the fluid and particles. In the presence of an electric field, the particles, due to an induced dipole moment, will form chains along the field lines. This induced structure changes the ERF's viscosity, yield stress, and other properties, allowing the ERF to change consistency from that of a liquid to something that is viscoelastic, such as a gel, with response times to changes in electric fields on the order of milliseconds. A good review of the ERF phenomenon and the theoretical basis for their behavior can be found in [Block and Kelly, 1988] and [Gast and Zukoski, 1989].

Control over a fluid's rheological properties offers the promise of new possibilities in engineering for actuation and control of mechanical motion. Any device that relies on hydraulics can benefit from ERF's quick response times and reduction in device complexity. Early development in practical applications of ERFs was hampered by the multidisciplinary approach required to understand them, which was not common. Today's scientists continue to improve upon ERFs, making them with more desirable properties. Their solid-like properties in the presence of a field can be used to transmit forces over a large range and have found a large number of applications [Duclos et al., 1992]. Devices designed to utilize ERFs include shock absorbers, active dampers, clutches, adaptive gripping devices, and variable flow pumps [Bullough et al., 1993; Choi, 1999]. An engineering application of ERF's is vibration control and a good review of the subject can be found in [Stanway et al., 1996].

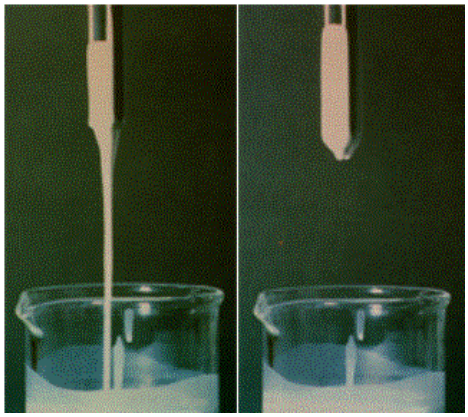

Figure 19: Electro-Rheological Fluid at reference (left) and activated states (right).

ERFs are generally recognized as behaving according to the Bingham plastic model for fluid flows, meaning that they will behave as a solid up to a certain yield stress. At stresses higher than this yield stress, the fluid will flow, and the shear stress will continue to increase with the shear rate, so that:

$$\tau = \tau_y + \mu\dot{\gamma} \tag{8}$$

where: τ is the shear stress, τ_y is the yield stress, μ is the dynamic viscosity and $\dot{\gamma}$ is the shear strain. The dot over the shear strain indicates its time derivative, the shear rate. In general, both the yield stress and the viscosity will be functions of the electric field strength.

An example of an ERF is the electro-rheological fluid LID 3354, manufactured by ER Fluid Developments Ltd., will be used [ER Fluids Developments Ltd, 1998]. LID 3354 is an electro-rheological fluid made up of 35% by volume of polymer particles in fluorosilicone base oil. It is designed for use as a general-purpose ER fluid with an optimal balance of critical properties and good engineering behavior. Solid and liquid are density matched to minimize settling. LID 3354 can be used in suitable equipment wherever electronic control of mechanical properties is required, such as in controlled dampers, actuators, clutches, brakes and valves. Its physical properties are: density: 1.46 x 10^3 kg/m^3; viscosity: 125 mPa.sec at 30°C; boiling point: > 200°C; flash point: >150°C; insoluble in water; freezing point: < -20°C.

The field dependencies for this particular ERF are:

$$\tau_{y,s} = C(E - E_o) \qquad \tau_{y,d} = AE^2 \qquad \mu = \mu_o - BE^2 \tag{9}$$

where: μ_o is the zero field viscosity; A, B, C and E_o are constants supplied by the manufacturer The subscripts s and d correspond to the static and dynamic yield stresses. The formula for static yield stress is only valid for fields greater than E_o. Figures 4 a, b, and c are a graphical representation of the last equations for the ERF LID 3354. Figure 4d shows the dependency of the current density at 30°C as a function of the field. Figure 4e shows the coefficient B of Equation (2) as a function of the temperature.

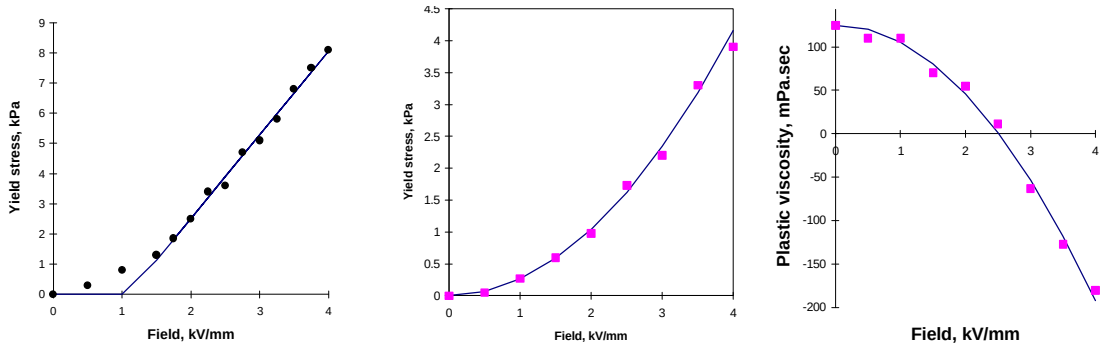

(a) Static Yield Stress at 30°C (b) DynamicYield Stress at 30°C (c) Plastic Viscosity at 30°C

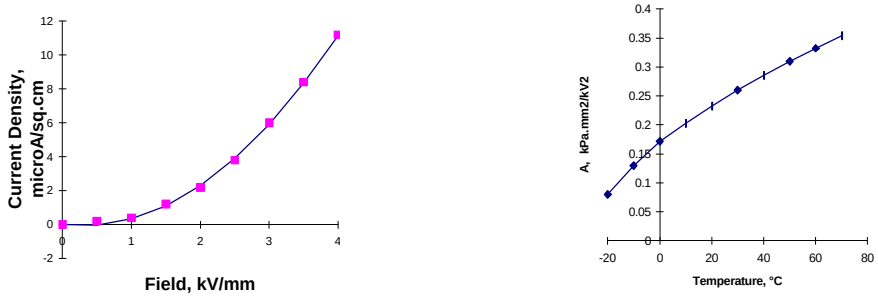

(d) Current Density at 30°C (e) Temperature Dependence of B,

Figure 20: Technical Information Diagrams for the ER Fluid LID 3354
[Published by Permission of ER Fluids Development Ltd]

The application of ERF's in robotic and haptic systems has been very limited. They have mainly been used as active dampers for vibration suppression [Furusho et al., 1997; Takesue et al., 1999]. In Virtual Reality and Haptic Systems, Electrorheological fluids have been proposed as tactile arrays to emulate the stiffness of remote/virtual objects [Taylor et al., 1996; Monkman, 1992]. Possible applications that have been considered are training purposes and Braille systems for the blind. Relatively large forces, small size, light weight and high bandwidth are the advantages of ERF's that make them very good candidates as actuators in robotic and haptic systems. However, there are two main disadvantages with these actuators that any designer should take into account: a) large voltages are required to produce the output forces and b) these actuators can only be used to emulate stiffness. This means that the output force is obtained as a reaction to an input force from a human operator or the environment. ERF's can not be used to apply "push" forces that will result in motion of a system.

5.1.5 REFERENCES

Binnard, M., 1995, *Boadicea: A Small Pneumatic Walking Robot*, Master of Science Thesis, Artificial Intelligence Laboratory, MIT.

Block, H. and Kelly, J. P., 1988, "Electro-Rhehology*", Journal of Physics, D: Applied Physics*, Vol. 21, pp. 1661.

Bullough, W. A., Johnson, A. R., Hosseini-Sianaki, A., Makin, J. and Firoozian, R., 1993, "Electro-Rheological Clutch: Design, Performance Characteristics and Operation," *Proceedings of the Institution of Mechanical Engineers, Part I, Journal of Systems and Control Engineering*, Vol. 207, No. 2, pp. 87-95.

Burdea, G., 1996, *Force and Touch Feedback for Virtual Reality*, John Wiley & Sons, Inc.

Choi, Seung-Bok, 1999, "Vibration Control of a Flexible Structure Using ER Dampers," *Transactions of the ASME, Journal of Dynamic Systems, Measurement and Control*, Vol. 121, pp. 134-138.

Dimarogonas, A., 1993, "The Origins of Machines and Mechanisms," in *Modern Kinematics, Developments in the Last Forty Years*, Edited by Erdman, A., John Wiley and Sons.

Duclos, T., Carlson, J., Chrzan, M. and Coulter, J. P., 1992, "Electrorheological Fluids – Materials and Applications," in *Intelligent Structural Systems*, Tzou and Anderson (editors), Kluwer Academic Publishers, pp. 213-241, Netherlands.

ER Fluids Developments Ltd, 1998, "Electro-Rheological Fluid LID 3354," *Technical Information Sheet*, United Kingdom.

Furusho J., Zhang G. and Sakaguchi M., 1997, "Vibration Suppression Control of Robot Arms Using a Homogeneous-Type Electrorheological Fluid," *Proceedings of the 1997 IEEE International Conference on Robotics and Automation*, Albuquerque, NM, pp. 3441-3448.

Gast, A. P., and Zukoski, C. F., 1989, "Electrorheological Suspensions as Colloidal Suspensions," *Advances in Colloid and Interface Science*, Vol. 30, pp. 153.

Gorbet, R., and Wang, D., 1998, "A Dissipativity Approach to Stability of a Shape Memory Alloy Position Control System", *IEEE Transactions on Control Systems Technology*, Vol. 6, No. 4, pp. 554-562.

Grant, D., 1995, *Shape Memory Alloy Actuator with an Application to a Robotic Eye*, Department of Electrical Engineering Thesis, McGill University, CA.

Grant, D. and Hayward, V., 1997, "Variable Structure Control of Shape Memory Alloy Actuators", *IEEE Control Systems Magazine*, Vol. 17, No. 3, pp. 80 – 88.

Henkenius, M., 1991, Electric Motor, *Popular Mechanics*, December 1991.

Hirose, S., Ikuta, K., and Umetani, Y., 1984, "A New Design Method of Servo-actuators Based on the Shape Memory Effect", *Theory and Practice of Robots and Manipulators, Proc. of RoManSy 1984, The Fifth CISM-IFToMM Symposium*, The MIT Press, Cambridge, MA.

Hirose, S., Ikuta, K. and Umetani, Y., 1989a, "Development of a Shape Memory Alloy Actuators. Performance Assessment and Introduction of a New Composing Approach," Advanced Robotics, Vol. 3, No. 1, pp. 3-16.

Hirose, S., Ikuta, K., and Sato, K., 1989b, "Development of a Shape Memory Alloy Actuator. Improvement of the Output Performance by the Introduction of a σ-Mechanism", *Advanced Robotics*, Vol. 3, No. 2, pp. 89-108, VSP and Robotics Society of Japan.

Hodgson, D., Wu, M. and Biermann, R., 1998, *Shape Memory Alloys*, http://www.sma-inc.com/SMAPaper.html.

Hollerbach, J., Hunter, I. and Ballantyne, J., 1992, "A Comparative Analysis of Actuator Technologies for Robotics," in O. Khatib, J. Craig and Losano-Perez Eds., *The Robotics Review 2*, MIT Press, Cambridge, MA, pp. 299-342.

Honma, D., Yoshiyuki, M., and Igushi, N., 1989, "Micro Robots and Micro Mechanisms Using Shape Memory Alloy," *Integrated Micro Motion Systems. Micro-machining, Control and Application*, Nissin, Aichi, Japan, The 3rd Toyota Conference.

Ikuta, K., Tsukamoto, M., and Hirose, S., 1988, "Shape Memory Alloy Servo Actuator System With Electric Resistance Feedback and Application for Active Endoscope", *Proc. of the 1988 IEEE International Conference on Robotics and Automation, Vol. 1.*, Computer Society Press, Washington, DC.

Ikuta, K., Tsukamoto, M., and Hirose, S., 1991, "Mathematical Model and Experimental Verification of Shape Memory Alloy for Designing Micro Actuator", *Proc. of the IEEE on Micro Electromechanical Systems, an Investigation of Microstructures, Sensors, Actuators, Machines, and Robots*, pp.103-108.

Kuribayashi, K., 1986, "A New Actuator of a Joint Mechanism Using Ti-Ni Alloy Wire", *The International Journal of Robotics Research*, Vol.4, No. 4, pp. 47-58.

Madill, D. and Wang, D., 1998, "Modeling and L2-Stability of a Shape Memory Alloy Position Control System", *IEEE Transactions on Control Systems Technology*, Vol. 6, No. 4, pp. 473-481.

Monkman, G. J., 1992, "Electrorheological Tactile Display", *Presence*, MIT Press, Vol. 1, No. 2.

Mosley, M., Mavroidis, C., and Pfeiffer, C., 1999, "Design and Dynamics of a Shape Memory Alloy Wire Bundle Actuator", *Proc. Of the ANS, 8th Topical Meeting on Robotics and remote Systems*, Pittsburgh, PA.

Mosley M. and Mavroidis C., 1999, “Experimental Non-Linear Dynamics of a Shape Memory Alloy Wire Bundle Actuator", submitted for publication in the *Proc. of the 1999 ASME Int. Mech. Eng. Congress and Exposition, Dyn., Measurement and Control Division*, Nashville, TE.

Reynaerts, D. and Van Brussel, H., 1991, "Development of a SMA High Performance Robotic Actuator," Proceedings of the Fifth International Conference on Advanced Robotics, Vol. 2, pp. 19-27, New York, NY.

Rosheim, M., 1994, *Robot Evolution: The Development of Anthrobotics*, John Wiley & Sons. Inc.

Schilling, 1999, http://www.schilling.com .

Spong, M., and Vidyasagar, M., 1989, *Robot Dynamics and Control*, John Willey & Sons.

Stadler, W., 1995, *Analytical Robotics and Mechatronics*, McGraw-Hill, New York.

Stanway, R., Sproston, J. L., and El-Wahed, A. K., 1996, “Applications of Electro-Rheological Fluids in Vibration Control: A Survey,” *Smart Materials and Structures*, Vol. 5, No. 4, pp. 464-482.

Stewart, H., 1987, *Pneumatics and Hydraulics*, revised by Tom Phibin, Macmillan Publishing Company, New York, 4th Edition.

Takesue, N., Zhang, G., Furusho, J. and Sakaguchi, M., 1999, "Precise Position Control of Robot Arms Using a Homogeneous ER Fluid," *IEEE Control Systems Magazine*, April 1999, pp. 55-61.

Taylor, P. M., Hosseini-Sianaki, A. and Varley, C. J., 1996, "Surface Feedback for Virtual Environment Systems Using Electrorheological Fluids," *International Journal of Modern Physics B*, Vol. 10, Nos 23 & 24, pp. 3011-3018.

Toki Corporation, 1987, *Biometal Guidebook*, Tokyo, Japan.

Troisfontaine, N., Bidaud, P. and Dario, P., 1997, "Control Experiments on Two SMA Based Micro-Actuators," *Proceedings of the Experimental Robotics (ISER 97)*, Barcelona, Spain.

Waram, T., 1993, *Actuator Design Using Shape Memory Alloys*, 2nd Edition.

Winslow, W. M., 1949, “Induced Fibrillation of Suspensions,” *Journal of Applied Physics*, Vol. 20, pp. 1137.

Zeldman, M., 1984, *What Every Engineer Should Know About Robots*, Marcel Dekker, Inc. .